POST IMAGE ACQUISITION MITIGATION OF EXCITATION LIGHT LEAKAGE IN PATTERNED ILLUMINATION BASED NIR FLUORESCENCE TOMOGRAPHY

M. Bartels,[†] *A. Joshi,*[†1] *J.C. Rasmussen,*[†] *W. Bangerth,*[*] *and E.M. Sevick-Muraca*[†]

[†]Department of Radiology, Baylor College of Medicine, Houston, TX 77030
[*]Department of Mathematics, Texas A&M University, College Station, TX 77840

ABSTRACT

Excitation light leakage through fluorescence filters limits the sensitivity of fluorescence tomography. We demonstrate an image processing approach for suppressing the effects of excitation light leakage from NIR fluorescence images. Multiple excitation and fluorescence emission wavelength images of a fluorescence target buried in $1\ \%$ Liposyn solution were acquired by scanning an intensity modulated and line shaped NIR excitation source over the illumination/detection surface of the tissue phantom. Excitation images were used to identify the NIR source pattern and multiple global and local filters were designed to mitigate excitation light leakage in the fluorescence images. The image correction approaches were assessed by comparing the processed fluorescence images with the output of an adaptive finite element based photon diffusion model. The results show that localized error modeling based on the median reduces leakage effects by about $44\ \%$ compared to uncorrected data.

Index Terms— Fluorescence optical tomography, excitation light leakage, frequency domain measurements

1. INTRODUCTION

Non-contact reflectance NIR fluorescence imaging and tomography [1] can be a powerful tool for molecular imaging of the biochemical environments of interest in clinically relevant volumes. Recently, the lymphatic system which is thought to be responsible for the metastatic spread of many cancers has been successfully imaged with NIR fluorescent agents including quantum dots and organic dyes [2, 3]. Due to the spatial spread of the potentially affected lymph nodes, fiber optic or raster scanned laser point excitation light delivery to tissue is not efficient for clinical applications such as sentinel lymph node mapping for tracking the spread of breast cancer. In breast cancer patients, the sentinel or the first lymph node draining the fluid from the primary tumor site could be located anywhere from axilla or clavicle (collar bone) to the sternum (chest wall) region. For conducting fluorescence imaging and tomography for lymph node localization, we proposed novel spatially patterned excitation light sources and demonstrated the increased information content of multiple patterned excitation based fluorescence measurements in a simulation study [4].

However the practical application of patterned excitation based NIR fluorescence tomography is currently impeded by the leakage of incident excitation light through the fluorescence filters, resulting in artifacts in the fluorescence images if the fluorescence signal is on the same scale as the excitation light leakage. Excitation light leakage can be remedied experimentally by employing collimation optics to improve optical filter performance [5], or alternatively the fluorescence images can be post-processed for leakage mitigation provided the structure of excitation light leakage artifacts is known. Both approaches are important open questions, and neither has been adequately addressed in the optical tomography community. This paper proposes a novel post-image acquisition approach for excitation leakage mitigation based on steady state excitation and emission images acquired during the homodyne frequency domain measurement process. We employ measurements acquired on a tissue mimicking phantom with an embedded fluorescent target. We compare local and global spatial filters employing an error and noise models based on excitation and emission images. The efficacy of the filters is validated by using an adaptive finite element based photon diffusion model to predict the fluorescence measurements on the tissue phantom.

2. MATERIALS AND METHODS

Experimental Setup. Fig. 1 depicts the experimental setup for frequency domain fluorescence image acquisition. A cube with $8\ cm$ sides was filled with $1\ \%$ Liposyn solution which mimics the optical properties of human breast tissue. A glass bulb of $9\ mm$ diameter filled with $1\ \mu M$ ICG dye was positioned at a depth of $1\ cm$ from the top surface. A line shaped excitation source was generated by placing a cylindrical lens in front of a $785\ nm$ laser diode, and mounting the entire assembly on a stepper motor; the source was then scanned across the surface. Images were acquired in a homodyne mode with a gain modulated image intensified CCD camera [6]. In this mode, the laser diode and the image intensifier are modulated at the same frequency ($100\ MHz$ in this

[1]Author contact: amitj@bcm.edu

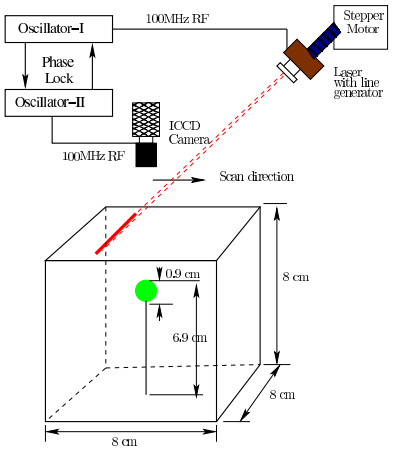

Fig. 1. *Experimental setup.*

case) via two phase locked oscillators with a constant phase offset. The phase offset is varied over a 2π cycle to collect steady state images corresponding to different phases. The complex fluorescence signal is then recovered by fitting a sine wave to the steady state images acquired for the full 2π cycle.

Five sets of images were acquired with the laser line source positioned at five discrete locations across the top surface of the tissue phantom. Sample excitation and emission images following phantom illumination with a scanning excitation source are depicted in Fig. 2. It is observed that when the line source is close to the fluorescent target, the constant excitation light leakage is dominated by the fluorescence signal, whereas the artifact in the fluorescence image is significant when the source is positioned away from the fluorescence target.

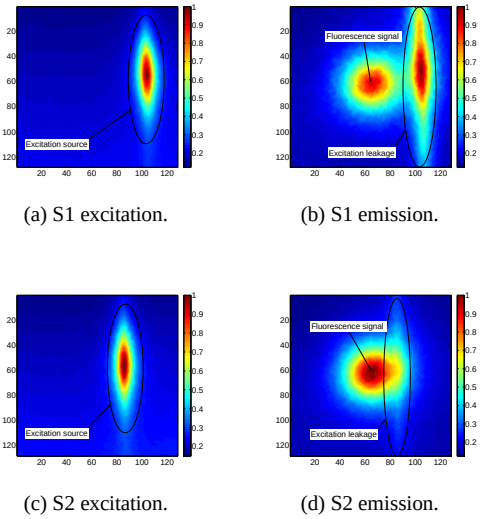

(a) S1 excitation. (b) S1 emission.

(c) S2 excitation. (d) S2 emission.

Fig. 2. *Normalized excitation (a,c) and emission (b,d) wavelength images for the scanning NIR laser source. The top* 8×8 *cm*^{2} *face of the phantom is imaged.*

Leakage removal framework. Fig. 3 depicts the framework for post-image acquisition leakage mitigation. The reduction of leakage takes places in the emission images. From the excitation images, prior knowledge on position and alignment of the leakage can be obtained as a linear feature. For orientation purposes, the length of the corridor is considered to be parallel to the alignment of the line source, whereas the width of the corridor is parallel to the scan direction. Knowing the leakage position, the error can be modeled and subtracted from emission. The loss of data in the emission image due to subtraction is replaced by adding Gaussian noise whose parameters are obtained from the original emission.

As the leakage is contained directly in emission images and may be of the same magnitude as the fluorescence signal, it cannot be isolated by simple techniques such as thresholding. In this study, we concentrate on leakage modeling. The line source position and its leakage are marked manually to obtain an affected corridor in the emission images. We then split the corridor into a set of lines parallel to the length of the corridor and separately correct each of them for leakage. To this end, we compute a single value for each line representing the intensity of suspected leakage light. In the final step, we replace each pixel value along the current line by the computed value. This provides an error model which can be subtracted from the original emission image to remove the leakage effect. Image correction can be applied locally only in the affected corridor, or globally to the entire emission image.

Many measures can be used to estimate the value which yields the error model. Below, we will compare the results from taking the arithmetic mean μ_a, median med, geometric mean μ_g, harmonic mean μ_h, trimmed mean μ_t and tri mean μ_3 as a measure [7]. Fig. 4 depicts error models for a local and a global corridor (*i.e.* two different corridor widths), as shown in Figs. 4(a) and 4(b), respectively. The x-axis represents the position of a line perpendicular to the corridor width. The y-axis expresses the computed estimate of leaked excitation for each line.

It can be seen from Fig. 4(a) that all measures model the leakage similarly. Hence, for scenarios where leakage is spatially isolated any of the models may be selected. However,

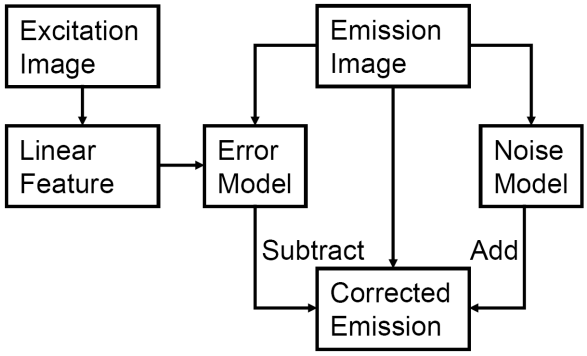

Fig. 3. *Leakage removal framework.*

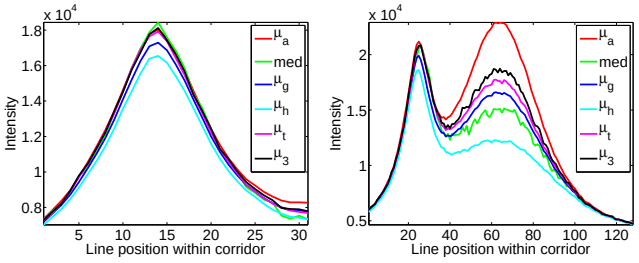

(a) Local error model. (b) Global error model.

Fig. 4. *Spatial error models: Statistical measures along vertical lines computed from Fig. 2(b).*

Fig. 4(b) suggests that in the global case leakage is properly modeled (narrow peak), however emission (broad peak) is also affected at the same time. Hence, subtraction of an error image from the emission images will remove the signal component as well as the leakage. This is particularly the case with μ_a since this measure is susceptible to high values such as the emission signal or noise.

After subtracting the modeled error from emission images, missing data needs to be replaced. It can be assumed that if isolated leakage was not present in the emission images, there would be noise in its place. A patch of noise in emission imagery is analysed, where no emission and excitation leakage is present. This patch can be found typically at the border of emission images, where it can be assured that there is neither emission nor excitation signal. This noise is Gaussian distributed with a particular mean, standard deviation and a range. These parameters are specific to the settings of the camera, image intensifier and the measurement environment. The modeled noise is added to the emission images after subtracting the modeled excitation leakage.

Forward Model. To study the impact of various global and local filter based image correction approaches, we generated simulated fluorescence emission measurements corresponding to the experimental setup, as described above. The excitation image defines the excitation source used to compute fluorescence levels, using optical absorption and scattering cross-sections of $1\ \%$ Liposyn taken from the literature, and quantum yield and lifetime of $1\ \mu M$ ICG filled in the glass bulb. The coupled frequency domain photon diffusion equations were solved on an adaptively refined mesh to predict the real and imaginary components of the fluorescence signal on the top surface of the phantom [1]. The model mismatch between predicted and experimentally measured fluorescence provides a measure of the efficacy of the excitation light mitigation strategies.

3. RESULTS AND DISCUSSION

The global and local excitation light leakage correction filters were applied to the raw emission images. Fig. 5 depicts the effect of global and local median filtering. It can be observed that while both filters remove similarly the majority of leakage artifact, the global filter affects the fluorescence signal all over the image, while the effect of the local filter is restricted to the linear corridor based on the excitation image.

In order to compare these corrected images with *true* emission levels, i.e. without any leakage, we simulated expected emission levels numerically. Fig. 6 shows the excitation and emission solutions on adaptively refined finite element meshes. Simulation starts with a coarse mesh with 64 hexahedral cells and is adaptively refined three times resulting in a mesh which is faithful to the distribution of line shaped source on the top surface of the phantom and spherical fluorescence source at $1\ cm$ depth. The simulated fluorescence fluence on the top surface of the finite element mesh is regridded into the same size as the experimentally observed CCD camera images of fluorescence to enable the comparison of simulated and experimental measurements.

Fig. 7 shows both real and imaginary components of fluorescence across the phantom surface as imaged on the CCD pixels, for both simulated (unaffected by leakage) and leakage-affected measurements. Individual pixels of the binned CCD images are treated as detectors. It can be observed that the match between simulation and experiment is satisfactory for the majority of CCD pixels. Leakage artifacts are confined primarily to the imaginary component of the fluorescence image, probably because of the phase mismatch between excitation and emission photon density waves.

Similar images can be generated for leakage-corrected experimental measurements. The mismatch between corrected or uncorrected experimental measurements u^e and simulated results u^s can then be quantified by defining the mean squared error $MSE = \frac{1}{N}\sum_{j=1}^{N}|u_j^s - u_j^e|^2$, where N is the number of detectors. Observation was made that the majority of global filtering techniques induce more errors than improving the quality of the images, as expressed by MSE, whereas local corrections reduce excitation light leakage without introducing further model mismatches. Fig. 8 compares the MSE for the two best filter results for the imaginary component, *i.e.* the global (red bars) and local (blue bars) leakage mitigation techniques against the uncorrected data (black bar). Only locally applied filters reduced the MSE to a substantial degree by $45.4\ \%$ and $43.6\ \%$ for local mean and local median, respectively. Finally, median filtering is preferred due to its robustness towards outliers.

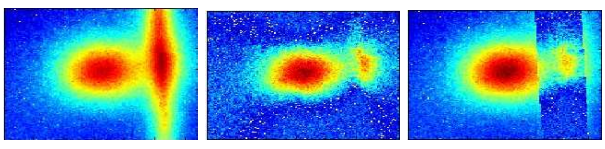

(a) Uncorrected. (b) Global filter. (c) Local filter.

Fig. 5. *Effect of applying the global and local median based correction to the raw emission image.*

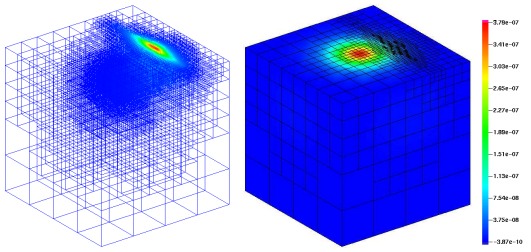

(a) Excitation. (b) Emission.

Fig. 6. *Adaptive finite element solution for the excitation and emission fluence for the scanning laser source and the experimental geometry described in Fig. 1.*

4. CONCLUSIONS AND FUTURE WORK

We have demonstrated post-image acquisition mitigation of excitation light leakage with global and local image processing filters for scanning excitation-based fluorescence imaging. Localized error modeling based on the median is promising as a reduction of about $44\ \%$ in the MSE between the processed experimental images and the simulated measurements was obtained. Further, this is the first time that scanning excitation source-based fluorescence measurements have been validated with a photon diffusion model on a known experimental setup. Our current and future work is focused on designing leakage removal filters with automated detection of excitation leakage artifacts by Hough transforms, and exploring the effects of leakage removal on the accuracy of inverse image reconstruction.

5. ACKNOWLEDGEMENTS

We would like to thank the anonymous reviewers for their constructive comments.

6. REFERENCES

[1] A. Joshi, W. Bangerth, K. Hwang, J. Rasmussen, and E. M. Sevick-Muraca, "Fully adaptive FEM based fluorescence optical tomography from time-dependent measurements with area illumination and detection," *Med. Phys.*, vol. 33, no. 5, pp. 1299–1310, 2006.

[2] S. Kim, Y. T. Lim, E. G. Soltesz, J. Lee A. M. De Grand, A. Nakayama, J. A. Parker, T. Mihaljevic, R. G. Laurence, D. M. Dor, L. H. Cohn, M. G. Bawendi, and J. V. Frangioni, "Near-infrared fluorescent type II quantum dots for sentinel lymph node mapping," *Nature Biotechnology*, vol. 22, pp. 93–97, 2004.

[3] R. Sharma, W. Wang, J. C. Rasmussen, A. Joshi, J. P. Houston, K. E. Adams, A. Cameron, S. Ke, S. Kwon, M. E. Mawad, et al., "Quantitative imaging of lymph function," *American Journal of Physiology- Heart and Circulatory Physiology*, vol. 292, no. 6, pp. H3109, 2007.

[4] A. Joshi, W. Bangerth, and E. M. Sevick-Muraca, "Non-contact fluorescence optical tomography with scanning patterned illumination," *Optics Express*, vol. 14, no. 14, pp. 6516–6534, 2006.

[5] K. Hwang, J. Houston, J. Rasmussen, A. Joshi, S. Ke, C. Li, and E. M. Sevick-Muraca, "Improved excitation light rejection enhances small animal fluorescent optical imaging," *J. Mol. Imaging*, 2005.

[6] J. S. Reynolds, T. L. Troy, and E. M. Sevick-Muraca, "Multi-pixel techniques for frequency-domain photon migration imaging," *Biotechnolgy Progress*, vol. 13, pp. 669–680, 1997.

[7] Bryan F. J. Manly, *Multivariate statistical methods: a primer*, Chapman & Hall, Ltd., London, UK, 3rd edition, 2005.

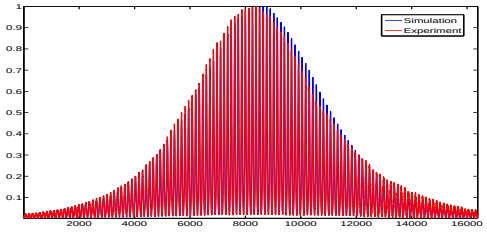

(a) Model mismatch: Fluorescence real component.

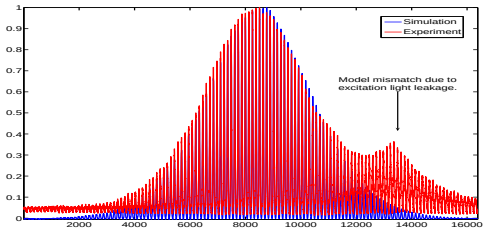

(b) Model mismatch: Fluorescence imaginary component.

Fig. 7. *Mismatch between experimentally observed and simulated fluorescence fluence on the phantom surface. The x-axis denotes the number of a CCD pixel, while the y-axis represents normalized magnitudes.*

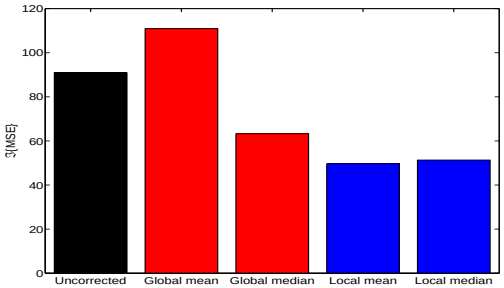

Fig. 8. *MSE between the simulated imaginary component of fluorescence fluence at the top surface and uncorrected and corrected measurements following the application of global and local excitation leakage filters.*